

Ultraviolet Raman Spectrometry

Sanford A. Asher

Reproduced from:

Handbook of Vibrational Spectroscopy

John M. Chalmers and Peter R. Griffiths (Editors)

© John Wiley & Sons Ltd, Chichester, 2002

Ultraviolet Raman Spectrometry

Sanford A. Asher

University of Pittsburgh, Pittsburgh, PA, USA

1 INTRODUCTION

Raman spectroscopy measures the magnitudes and intensities of frequency shifts that occur because of the inelastic scattering of light from matter.^{1–4} The observed shifts can be used to extract information on molecular structure and dynamics. In addition, important information can be obtained by measuring the change in the electric field orientation of the scattered light relative to that of the incident exciting light.

The experiment is usually performed by illuminating a sample with a high-intensity light beam with a well-defined frequency and a single linear polarization (Figure 1); the scattered light is collected over some solid angle and measured to determine frequency, intensity, and polarization. The inelastic scattering Raman phenomenon, which leads to frequency shifts, is phenomenologically distinct from the relaxed emission denoted as fluorescence (Figure 2) because the inelastic scattering is a single event, and a real emitting excited state is never created.

In contrast, relaxed fluorescence emission (Figure 2) occurs through the population of an excited state, which can subsequently undergo vibrational relaxation prior to fluorescence back to the ground state. The distinction between fluorescence and Raman scattering is more subtle for excitation within the absorption bands of small molecules in the gas phase, where single vibrational-level fluorescence can occur from well-defined vibronic levels.⁵

Much of the early work centered on vibrational Raman scattering; these studies were central to developing a fundamental understanding of molecular structure and vibrational motion. Before 1945 it was much easier to take Raman spectroscopic measurements than to take

mid-infrared absorption measurements. Raman excitation used Hg arc emission lines and photographic detection. The use of the Hg arc allowed the first ultraviolet (UV) Raman measurements, some of which were actually resonance Raman measurements within the absorption bands of analyte molecules.

After 1945 the advent of relatively convenient IR instrumentation decreased enthusiasm for Raman spectroscopy, and it became a specialized field. Much of the work before 1960 centered on examining molecular structure and molecular vibration dynamics. Major advances occurred during this period in the theoretical understanding of Raman spectroscopy and in the resonance Raman phenomenon, where excitation occurs within an electronic absorption band. The first commercial Raman instrument became available in 1953.

The advent of the photomultiplier tube and the He–Ne laser caused a resurgence of interest. In 1928, 58 papers were published on Raman spectroscopy; by 1937, the total was 1785. Between 1987 and 1989, for example, more than 6000 papers were published with the word Raman in their title.⁶ Raman spectroscopy has become a major tool for fundamental studies in physics and physical chemistry as well as for applied studies in the biological sciences and analytical chemistry.

During the 1970s most Raman instrumentation used Ar⁺ lasers with excitation between 450 and 520 nm – a region that, unfortunately, is especially prone to interference from fluorescent impurities. The interferences degrade signal-to-noise ratios (S/Ns), resulting in poor spectra for many complex samples. Many Raman studies involved pure compounds or those samples that proved amenable to visible excitation.

The usefulness of Raman spectroscopy for studying aqueous samples, especially biological samples, was

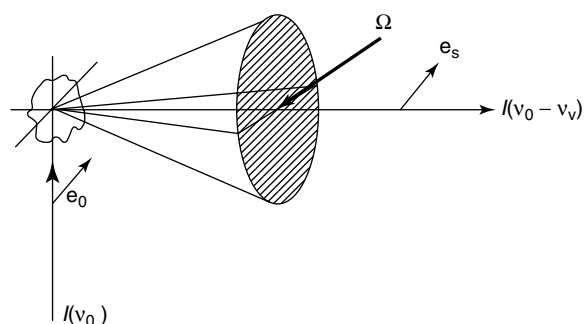


Figure 1. Raman inelastic light-scattering process showing excitation of a sample with light of an intensity $I(\nu_0)$ and frequency ν_0 . The incident light has an electric field of magnitude and direction shown by \mathbf{e}_0 . Raman scattered light at a frequency $\nu_0 - \nu_v$ (ν_v is the Raman active molecular vibrational frequency) and intensity $I(\nu_0 - \nu_v)$ is collected over the solid angle Ω . A ray of this light is shown with its electric field polarized along \mathbf{e}_s parallel to the incident field. [Reprinted with permission from S.A. Asher, *Anal. Chem.*, **65**(2), 60A (1993). Copyright © (1993) American Chemical Society.]

appreciated early on. Because the Raman scattering of water is very weak, it is easy to study species in aqueous environments. IR measurements, in contrast, often suffer from water interferences that cannot be overcome. In 1972 a paper by Streckas and Spiro⁷ demonstrated the usefulness

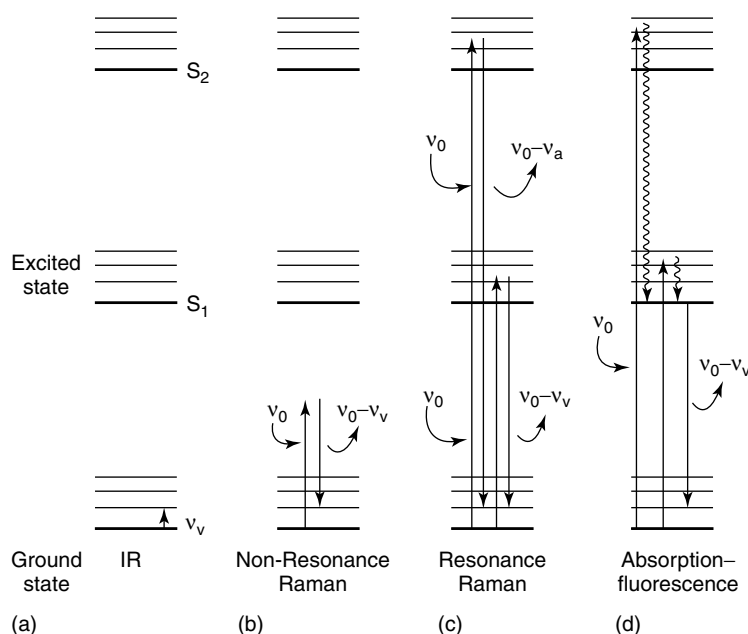


Figure 2. Infrared (IR) absorption and Raman scattering. (a) Vibrational IR absorption. (b) Inelastic scattering of light of frequency ν_0 to a frequency of $\nu_0 - \nu_v$. The shift in frequency corresponds to a vibrational frequency in this case, and the scattering is known as vibrational Raman scattering. Because the excitation occurs at a frequency far removed from any absorption bands associated with excitations to electronic excited states, the phenomenon is known as normal, or non-resonance, Raman scattering. (c) Excitation occurring within an electronic transition produces resonance Raman scattering. (d) Absorption and fluorescence emission in which an excited state is created. Typical relaxed fluorescence occurs subsequent to the population of an excited state. Prior to emission, this excited state quickly relaxes to the lowest vibrational level of the lowest singlet excited electronic state. Emission is broad and the molecule undergoes a transition to different vibronic levels of the ground state. [Reprinted with permission from S.A. Asher, *Anal. Chem.*, **65**(2), 60A (1993). Copyright © (1993) American Chemical Society.]

of the resonance Raman effect in selective studies of the chromophoric hemes of hemoglobin and myoglobin. Spectra of very high S/N were obtained from heme protein samples at relatively low concentrations. This technique was quickly adopted by those researchers interested in biological problems. Amazing progress has been made over the past 30 years using this technique to, for example, study heme protein structure and function^{8,9} and to elucidate the photochemical mechanisms of visual pigments such as rhodopsin.¹⁰ Until recently, however, resonance Raman spectroscopy was limited to the small subset of compounds absorbing in the visible or near-UV spectral regions where laser sources typically have been available.

The 1980s saw even more rapid advancements, such as the development of UV-Raman spectroscopy and of Fourier transform (FT)-Raman spectroscopy,¹¹ which uses near-infrared excitation. These extensions into spectral regions away from the visible have dramatically increased the utility and applicability of Raman spectroscopy.

In FT-Raman spectroscopy, the multiplex advantage of the Michelson interferometer is used to increase the spectral S/N that is limited by IR detector background noise. FT-Raman spectroscopy has the advantage of excitation in a spectral region that is much less susceptible

than visible excitation to fluorescent interferences. Non-resonance Raman measurements of samples result in Raman vibrational intensities that are roughly proportional to concentrations of those species in the sample; the Raman-active vibrations have roughly similar intensities. For example, aromatic ring vibrations have intensities similar to those of aliphatic C–C stretching vibrations, which have intensities similar to those of C–H stretching vibrations.

In contrast, UV-Raman spectroscopy uses selective excitation in the UV absorption bands of molecules to produce spectra of particular analytes and chromophoric segments of macromolecules. Resonance excitation has the advantage of selectivity. In addition, UV-Raman measurements of condensed-phase samples excited below 260 nm are not plagued by fluorescent interferences.¹²

2 PHENOMENOLOGY

Figure 3 illustrates the Raman scattering phenomenon. An incident electromagnetic field drives the electron cloud of the molecule at the incident frequency ν_0 . An oscillating dipole moment is created by the resulting displacement of electronic charge. Because the charge is accelerating, it radiates energy in the form of electromagnetic radiation. The radiated frequency ν_0 is identical to the excitation frequency; light is scattered elastically. If the scattering species is small compared with the wavelength of light, the scattering is known as Rayleigh scattering. Because charge acceleration induces the radiation, the Rayleigh scattering efficiency increases with the fourth power of the excitation frequency. This phenomenon explains why the sky is blue and the setting (or rising) sun is red.

Other dynamic processes modulate the induced oscillating dipole moment. As shown in Figure 3, a nuclear

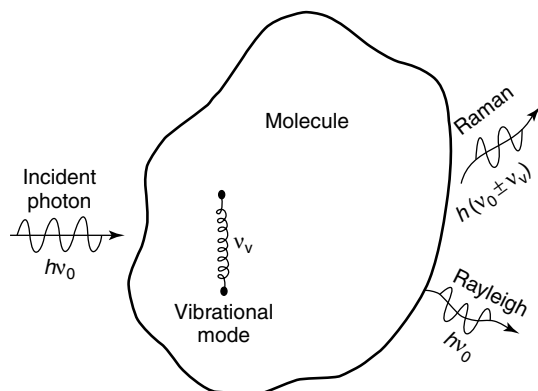


Figure 3. Raman scattering phenomenon. The presence of a vibration at frequency ν_v is shown by the spring. Light scattered at $\nu_0 - \nu_v$ is known as Stokes Raman scattering; light scattered at $\nu_0 + \nu_v$ is known as anti-Stokes Raman scattering. [Reprinted with permission from S.A. Asher, *Anal. Chem.*, **65**(2), 61A (1993). Copyright © (1993) American Chemical Society.]

vibrational motion causes an oscillation of the electron cloud at frequency ν_v . The electron cloud oscillation at ν_0 couples to the vibrationally induced electron cloud oscillation at ν_v to give rise to a beat oscillation at $\nu_0 \pm \nu_v$, which radiates Raman scattered light at this frequency. Those vibrations that most efficiently Raman scatter are those that couple most effectively to the oscillating electric dipole moment induced by the exciting electromagnetic field.

There are particular excitation frequencies that are natural frequencies of oscillation of specific electron oscillators of the molecular electron cloud. These natural frequencies are the molecular electronic absorption band frequencies. Excitation at these frequencies is said to be in “resonance” with the electronic transition (Figure 2); therefore, the Raman scattering is said to be “resonance Raman” scattering. This resonance excitation at the natural frequency of electron cloud oscillation results in an increased oscillating charge displacement and a corresponding increase in the induced dipole moment; this, in turn, results directly in an increased scattering or reradiation efficiency for Raman scattering. The enhancement factor of resonance Raman scattering compared with that of normal Raman scattering can be as high as 10^8 .

The observed Raman band intensities at a particular excitation frequency depend on the degree to which a vibration modulates the molecular polarizability. Classically, the magnitude of the induced dipole moment μ depends linearly on the molecular polarizability α and the incident electromagnetic field \mathbf{E} , giving $\mu = \alpha\mathbf{E}$. In the case of Raman scattering, the effective polarizability is not the static polarizability α ; it is the Raman polarizability α^R associated with perturbation of the static polarizability by the Raman active vibration $\alpha_R = (\partial\alpha/\partial Q)_0 Q$, where Q is the normal vibrational mode displacement. For excitation at frequency ν_0 , the Raman intensity I_{mn} observed over a unit solid angle for a transition between vibronic levels m and n in the electronic ground-state manifold is¹³ $I_{mn} = \sigma^R N I_0 W(\Omega)$, where σ^R (cm^2 per molecule sr^{-1}) is the total differential Raman cross-section for a single gas-phase molecule integrated over the Raman peak bandwidth, I_0 is the incident excitation intensity (photons $\text{cm}^{-2} \text{s}^{-1}$) into a particular sample volume element of area dA and length dl , N is the number of molecules within that volume element, and $W(\Omega)$ is a parameter that details the optical geometry and includes factors such as the collected solid angle Ω and the spectrometer efficiency.

The resonance Raman effect can lead to important selectivity in Raman spectral measurements. Figure 4 shows the absorption spectrum of a sample with two absorption bands. Raman spectra are shown that are excited at a wavelength longer than any absorption band (normal Raman) or within the two absorption bands (resonance Raman).

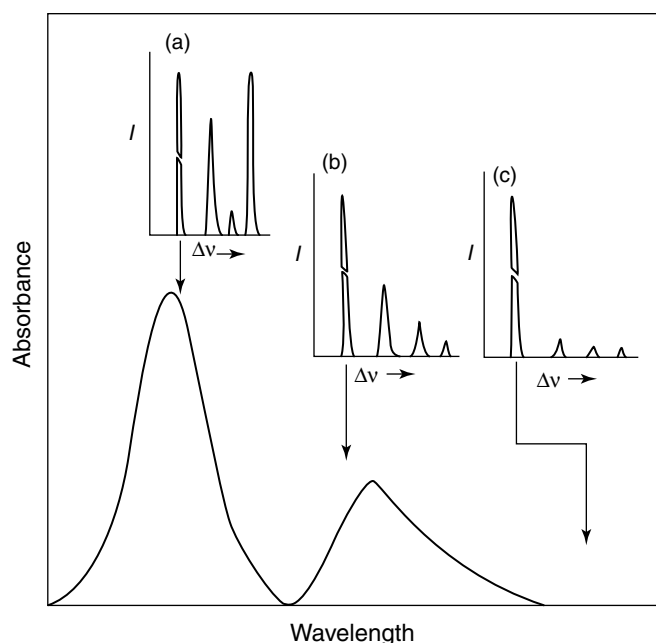


Figure 4. Selectivity available from resonance Raman spectroscopy. The absorption spectrum is shown for a sample with two absorption bands. These bands could derive from two different analytes, two different chromophoric segments of a macromolecule, or two different electronic transitions of a single molecule. Three different Raman spectra are shown that derive from resonance Raman excitation within either of the two absorption bands (a and b) or from excitation away from the absorption (c). Excitation within resonance leads to much more intense Raman spectra. The most intense feature is the Rayleigh scattering band. [Reprinted with permission from S.A. Asher, *Anal. Chem.*, **65**(2), 62A (1993). Copyright © (1993) American Chemical Society.]

Excitation away from resonance results in comparable Raman intensities from all analytes. The typical scattering cross-section is $\sigma^R = 10^{-30} \text{ cm}^2$ per molecule sr^{-1} (or $1 \text{ } \mu\text{b}$ per molecule sr^{-1} , where 1 b equals 10^{-24} cm^2). Resonance excitation within an absorption band can lead to an immense Raman intensity increase. For example, we have measured a Raman cross-section of $\sim 50 \text{ b}$ per molecule sr^{-1} for pyrene.¹⁴

Figure 4 shows an increased Raman intensity occurs for resonance excitation. Different Raman spectra are observed with excitation in resonance versus not in resonance. In addition, different spectra are observed with resonance excitation within different sample absorption bands. If these absorption bands derive from different analytes in the sample, we selectively enhance the vibrational Raman spectrum of different analytes as we change the excitation wavelength. The selectivity factor can be as large as 10^8 .

If the different absorption bands derive from different segments of a molecule, by changing excitation wavelengths we change the segment of the molecule studied. In contrast, if the two absorption bands derive from the same

chromophoric segment of a single molecule, the spectra will differ because of differences in the structure of the excited states associated with the two electronic transitions; the different excited states couple differently with the ground-state vibrational motion.

We can easily estimate the number of non-resonance Raman photons that can be detected from a 0.1 M solution of an analyte with a Raman cross-section of $1 \text{ } \mu\text{b}$ per molecule sr^{-1} , illuminated by an incident laser beam of 1 W of 514.5 nm light (2.6×10^{18} photons s^{-1}). For a typical case, the limiting aperture is the height of the intensified Reticon detector (2.5 mm), and the spectrometer $f/\#$. Let us assume the spectrometer is $f/7.0$, with a slit width of $200 \text{ } \mu\text{m}$, and the collection optic has a magnification of 6. For this case, the laser beam can be efficiently imaged into a column with a $33\text{-}\mu\text{m}$ (maximum) diameter and a $417\text{-}\mu\text{m}$ height that contains 2.2×10^{13} molecules. Ideally, we can collect 0.86 sr of the scattered light. According to the equation, if the spectrometer were 100% efficient, a total of 5.6×10^6 Raman photons s^{-1} would be detected for this vibration.

In contrast, the fluorescence cross-section of an analyte with a molar absorptivity of 10^4 and a fluorescence quantum yield of 0.1 is equal to $3 \times 10^{-19} \text{ cm}^2$ per molecule sr^{-1} ; $\sim 2 \times 10^{18}$ fluorescence photons would be observed using the same instrument (assuming no self-absorption of the emitted light occurs).

Obviously, the fluorescence experiment is much more sensitive than the Raman experiment and we can observe the same amount of fluorescence signal as the Raman signal using a concentration $\sim 3 \times 10^{11}$ -fold lower. However, in the case of resonance Raman scattering, Raman cross-sections as high as $\sim 10^{-22} \text{ cm}^2$ per molecule sr^{-1} can occur. The resonance Raman sensitivity, while always smaller, can approach within a 1000-fold that of fluorescence. Furthermore, the combination of selectivity and sensitivity can be greater because the Raman spectra have higher resolution.

Generally, numerous Raman bands exist, and all can be used to determine concentrations. The narrow Raman spectral bands carry a great deal of information on molecular structure, in contrast to the broad fluorescence emission. Also, the Raman cross-sections are much less dependent on environment than are the fluorescence quantum yields. Modest changes in solvent composition can cause dramatic changes in fluorescence quantum yields, because the quantum yields are very sensitive to relatively small changes in fluorescence lifetimes. Thus, resonance Raman measurements can be very sensitive, the spectra can provide a great deal of molecular structural and environmental information, and an increased selectivity results from the ability to excite particular species.

3 INSTRUMENTATION

UV-Raman instrumentation has evolved rapidly. The original laser source used a low repetition rate (20 Hz) neodymium doped yttrium aluminum garnet (Nd:YAG) laser with ~ 5 -ns frequency pulses that were doubled or tripled to pump a dye laser whose frequency was doubled or mixed with the Nd:YAG 1.06- μm fundamental wavelength to generate light between 200 and 400 nm.^{15,16} The minimum average output power available in this region is 20 mW; in some spectral regions, hundreds of milliwatts are available. Raman shifting of the Nd:YAG harmonics in H₂ gas can also generate numerous wavelengths in the UV, and this approach can be used to construct a simpler, inexpensive UV laser source.

The low-duty cycle (10^{-7}) of the Nd:YAG laser represents a major limitation because the laser pulses cannot be focused into a sample volume that can be efficiently imaged into the Raman spectrometer. The Nd:YAG output occurs as ~ 5 ns pulses, at a repetition rate of ~ 20 Hz. An average power of 20 mW corresponds to a peak power level of ~ 200 kW, which can induce nonlinear optical phenomena in matter. A power flux value of 2.5 GW cm^{-2} would occur if this beam were focused into a 100- μm -diameter spot size.

A partial solution to this low-duty cycle is to use a higher repetition rate YAG laser and to Raman shift it into the UV. The high temporal and spatial mode structure of the Coherent Infinity 100 Hz YAG lasers results in extremely efficient harmonic generation and H₂ Raman shifting.

Another approach is to use high repetition rate excimer lasers to directly pump a dye laser whose output can be frequency doubled into the UV region.¹⁷ High-power excimer lasers can have repetition rates between 200 and 500 Hz; at the highest repetition rates the 16-ns laser pulses result in a duty cycle of 8×10^{-6} . This partially alleviates the nonlinear optical phenomena and the sample ground-state depletion¹⁸ that both complicates the Raman spectral measurements and necessitates defocusing the laser excitation beam at the sample. An alternative approach uses a mode-locked Nd:YAG laser to create a quasi-continuous wave (CW) UV source with a duty cycle of 0.01.^{19,20} A new tunable quasi-CW UV laser source has been demonstrated that utilizes a titanium sapphire laser that is frequency quadrupled to generate light tunable from 205 to 230 nm.²¹

True CW UV laser excitation can now be obtained by intracavity doubling of Ar and Kr lasers. The intracavity Ar laser gives five excitation wavelengths in the UV region: 257, 248, 244, 238, and 228.9 nm,²² while an intracavity doubled Kr laser gives 206-nm light.²³ These lasers give rise to a major improvement in spectral S/N and, for the first time, allow UV-Raman studies of solid absorbing samples.

The major difficulty with these laser sources is that they are large and expensive. A new hollow cathode UV laser has recently been demonstrated that utilizes sputtered silver or copper in a noble gas to give rise to 224-nm and 248-nm excitation.²⁴ The output is quasi continuous at 1 kHz with a duty cycle of $\sim 1\%$. The advantage of this laser is that it is small and inexpensive ($< \$10 \text{ K}$), it is air-cooled and it has a low power consumption.

UV-Raman sample handling requires flowing the sample through the laser beam as a liquid jet, through a capillary, or along a waveguided stream. With pulsed lasers, it is essential to exchange each illuminated sample volume before the arrival of the next laser pulse to avoid sample heating; also, the high-energy UV photons might cause photochemical degradation in the samples. Most samples studied to date have not shown significant monophotonic photodegradation during the typical 10-min Raman measurement time.

The collection optics use either an ellipsoidal collection mirror^{15,16} for achromatic imaging or quartz lenses (when accurate relative intensity measurements are not essential). The typical spectrometer is a triple grating instrument in which the initial double monochromator operates in a subtractive configuration to filter out the Rayleigh scattered light. The third-stage spectrograph disperses and images the light onto a multichannel detector such as an intensified Reticon array. This multichannel detector is essential for simultaneous collection of the entire spectrum. A scanning system would have a far inferior S/N because most of the noise comes from the low-stability UV laser source. Intensified charge-coupled device (CCD) detectors have proven to be superior to the intensified Reticon detectors.

The triple spectrometer is inefficient; at best, only 7% of the Raman scattered light entering the entrance slit is transferred to the detector. We recently developed a highly efficient new single grating UV-Raman spectrometer, which utilizes dielectrically coated mirrors and a dielectrically coated long pass filter to remove the Rayleigh scattered light.²⁴ The spectrometer utilizes a solar blind intensified CCD detector to optimize signal to noise. We further developed an efficient UV-Raman microscope spectrometer for studying small sample areas.²⁵

4 FUNDAMENTAL APPLICATIONS

Investigations of the structure and dynamics of excited states of small molecules are an especially fertile area for UV-Raman investigations. Examination of the vibrations most enhanced by excitation in resonance with an electronic transition gives information on the excited-state structure and dynamics. The simplest rule of thumb

is that resonance Raman-enhanced vibrations are those that distort the ground-state geometry toward the excited-state geometry. If the atomic motions involved in the enhanced vibrations are known, theoretical models can be applied to the measured Raman intensities to calculate the excited-state distortion. Numerous workers are using this approach to examine the excited states of small molecules such as oxygen,²⁶ ammonia,²⁷ methyl iodide,^{28,29} carbon disulfide,³⁰ ethylene,^{31–33} and other species.

For methyl iodide,^{28,29} the excited state is dissociative and the Raman data give information on the short time dynamics of the photodissociation. For ethylene, excitation in the lowest allowed $\pi \rightarrow \pi^*$ transition results in the unique enhancement of the overtone of a torsional vibration, in addition to the C=C double-bond stretch and the CH₂ bending vibration; the enhancement of this torsional vibration confirms that the ethylene excited state is twisted.^{32,33} Similar experiments examine the vibrational enhancement of stilbenes,^{32,33} for example, to determine the photochemical mechanism of photoisomerization. Interested readers are urged to examine the rapidly expanding literature on these insightful studies.

UV-Raman spectroscopy has been applied extensively to biological molecules, especially to probe the structure and function of proteins. Early applications explored the excited states of aromatic amino acids, nucleic acids and amides.³⁴ For example, recent studies examined the excited states of amides in order to determine the origin of the resonance Raman enhancement mechanism.^{34–36} To investigate the prototypical amide bond, Asher *et al.* examined the resonance Raman enhancement mechanism in *N*-Methylacetamide (NMA).

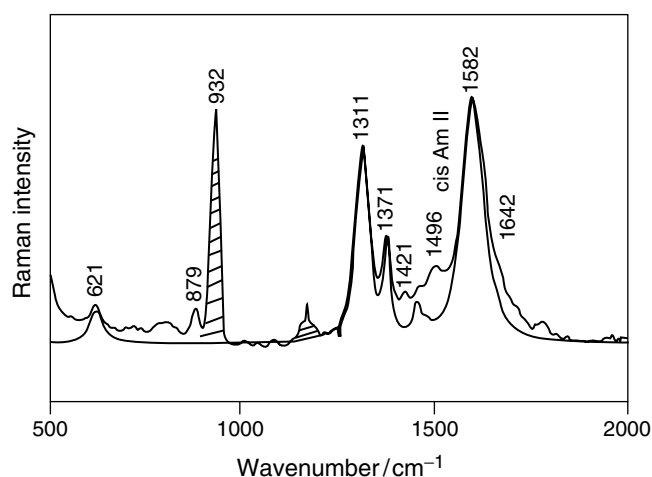


Figure 5. Comparison of the measured and calculated 218 nm excited spectrum of trans ¹³CH₃CONHCH₃ in water (42 mM). See text for details. [Reprinted with permission from S.A. Asher, *J. Am. Chem. Soc.*, **117**(10), 2893 (1995). Copyright © (1995) American Chemical Society.]

Figure 5 compares the theoretically calculated and the measured UV-Raman spectrum for the ¹³C_α isotope of NMA. The major features include a weak 1642 cm⁻¹ shoulder for the amide I vibration, strong 1582 and 1311 cm⁻¹ bands for the amide II and III vibrations, and a moderate-intensity 1371 cm⁻¹ CH₃ umbrella mode band. The other differences observed derive from the lack of an internal standard band at 932 cm⁻¹ and the lack of a cis NMA component at 1495 cm⁻¹.

This theoretical study found that the amide excited state was mainly expanded along the C(O)–N bond, with a smaller expansion along the C=O bond and with smaller contractions along the C–C(O) and N–C bonds. In the case of diglycine derivatives they discovered that the lowest-energy electronic transition was a charge transfer transition from the carboxylate to the amide bond.^{37–39} This accounted for the anomalous enhancement of carboxylate stretching vibrations for the penultimate carboxylates of proteins and peptides.

5 ANALYTICAL APPLICATIONS

The ability of UV resonance Raman spectroscopy to selectively examine the vibrational spectra of particular species in complex mixtures makes the technique uniquely important for analytical applications. Selectivity is determined by the relative Raman cross-sections of the analyte compared with other species present in the sample. Sensitivity depends on the magnitude of the analyte Raman cross-sections compared with those of overlapping, interfering Raman bands and emission from the sample. Fluorescence interference does not normally occur in condensed phases with UV excitation below 260 nm; those species with their lowest singlet states below 260 nm have vanishingly low fluorescence quantum yields because they are flexible and return to the ground state through nonradiative processes.¹²

Polycyclic aromatic hydrocarbons (PAHs) are the most intense Raman scatterers.^{40–43} The UV-Raman spectra of a series of PAHs in Figure 6 show numerous bands that are indicative of fused-ring systems. The vibrations that are enhanced are mostly symmetric in-plane ring-breathing vibrations. The spectra, though similar, differ enough to identify the ring system. Although aliphatic ring substituents perturb the spectra, the enhanced vibrations remain predominantly ring-breathing modes; peripheral substituent vibrations are not generally observed unless they are conjugated into the aromatic π network.⁴⁰ The major changes that occur upon ring substitution involve alterations in relative intensities and frequency shifts, which depend on the substitution patterns in the different compounds. The Raman cross-sections are large enough that it is easy to study these

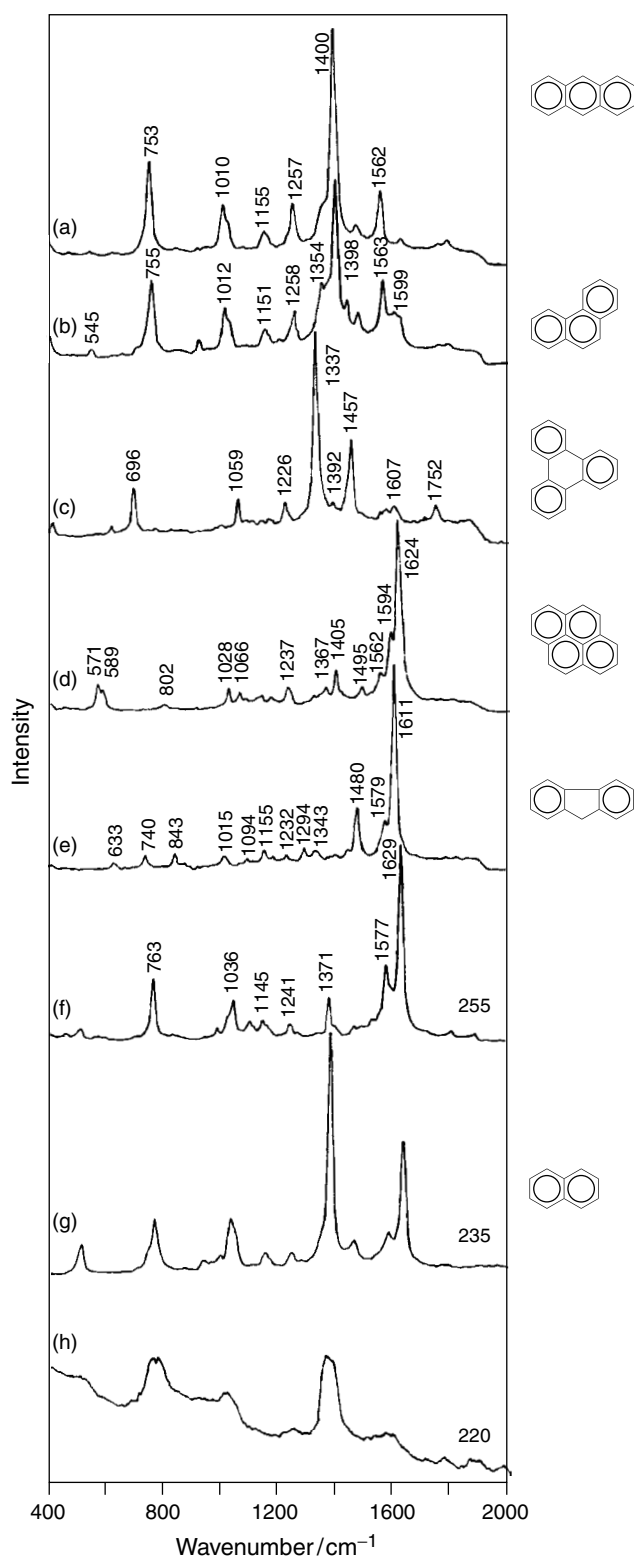


Figure 6. Resonance Raman spectra of 5 mM solutions of PAHs dissolved in acetonitrile and excited at 255 nm. (a) Anthracene. (b) Phenanthrene. (c) Triphenylene. (d) Pyrene. (e) Fluorene. Naphthalene excited at (f) 255 nm, (g) 235 nm, and (h) 220 nm. [Reprinted with permission from S.A. Asher, *Anal. Chem.*, **65**(4) (1993). Copyright © (1993) American Chemical Society.]

analytes at parts per million (ppm) and parts per billion (ppb) and even parts per trillion (ppt) concentrations.^{40,43}

The large cross-sections of these compounds has allowed the Stair group to use UV-Raman to study coke formation in catalysts such as ZSM-5 and USY zeolites.^{44,45} They were able to selectively examine the formation of PAHs and demonstrated the selective formation of PAHs on USY zeolites.

Similarly the Asher group demonstrated the ability to selectively study non-diamond carbon in chemical vapor deposition (CVD) diamond-grown films.^{23,46-48} They constructed a UV-Raman microscope to examine the spacial distribution of non-diamond carbon in these CVD films. They found that the non-diamond carbon localized at the interstices between diamond crystallites.²⁵ The Raman spectra of diamond show high S/Ns with UV excitation below 229 nm. Excitation at 206 nm showed strong first-order and higher-order Raman bands. In addition, strong narrow luminescent bands from defects were also observed. The intensities were sufficiently high that monolayer coverage of diamond could be observed on a silicon substrate.

On the basis of the high signal-to-noise spectra the Asher group constructed a UV-Raman spectrometer to examine in situ the growth of diamond in a microwave plasma CVD diamond reactor (Figure 7). A 1.5-kW ASTeX microwave plasma reactor was used for CVD diamond growth. The in situ UV-Raman spectra were excited with a 244-nm light beam, which was expanded and focused onto the growth substrate/sample inside the reactor.

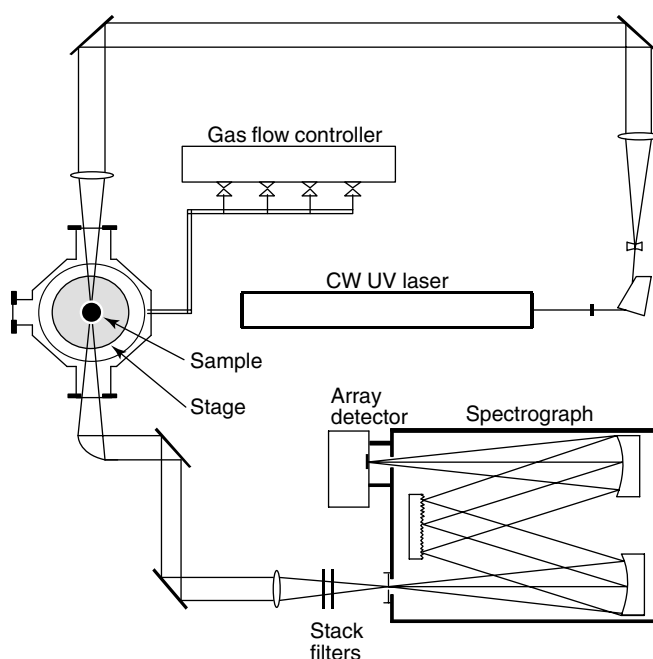


Figure 7. Schematic diagram showing the UV-Raman spectrometer coupled to the ASTeX plasma CVD diamond growth chamber.

The scattered light was collimated by using a parabolic mirror. Two 244-nm dielectric stack filters were used to reject Rayleigh scattering and the Raman scattered light was reimaged onto the slit of a modified Spex 1701, single monochromator and detected by an intensified photodiode array. Approximate confocal imaging was used to help minimize interference from the plasma emission in the reactor. Although the plasma emission intensity in the visible is sufficiently high to prevent Raman measurements, it decreases dramatically in the UV spectral region at ~ 260 nm.

Figure 8 shows the temperature dependence of the first-order Raman band of the growing diamond films (~ 1332 cm^{-1} at room temperature). We see very high S/N

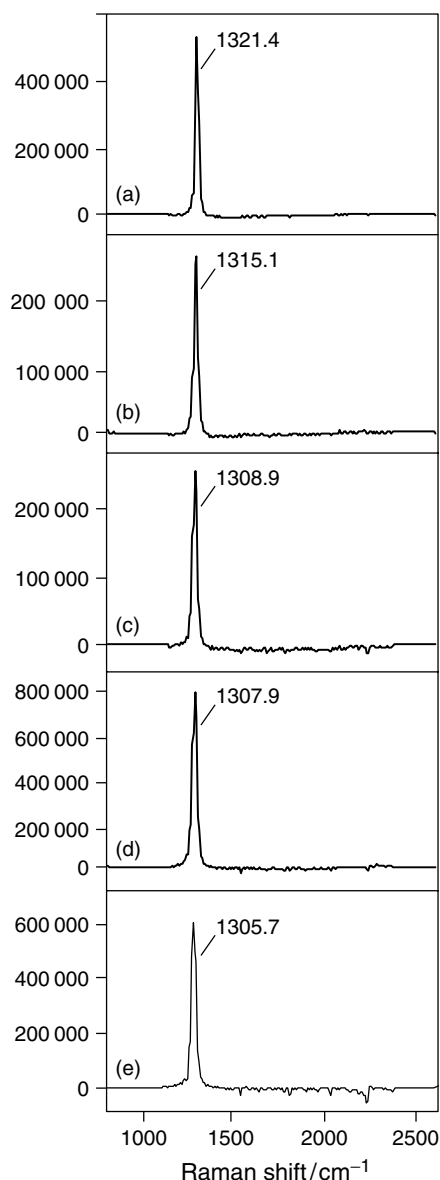


Figure 8. Temperature dependence of the in situ 244-nm UV-Raman spectra of CVD diamond films grown within the plasma reactor: (a) 578 °C; (b) 766 °C; (c) 930 °C; (d) 955 °C; (e) 1008 °C.

spectra for relatively short ~ 10 min spectral accumulation times. We calculate that the detection limit for the growing CVD diamond films is a film of ~ 0.8 nm thickness.

The spectra display the well-known frequency decrease of the ~ 1332 cm^{-1} first-order phonon band with temperature. We were surprised to see no non-diamond carbon impurity bands in these spectra since they were clearly observed in spectra of these same CVD films when they were cooled down to room temperature. We discovered that these non-diamond carbon bands are enhanced by a narrow electronic resonance whose frequency is temperature dependent. This electronic resonance shifts away from this 244-nm excitation wavelength at elevated temperatures.

The use of UV-Raman for remote detection of chemical species has recently been demonstrated by the construction of a UV-Raman Lidar system for studying organic species remotely in the atmosphere and on surfaces.^{49,50} This Lidar system used a telescope and 266-nm excitation from a quadrupled YAG laser. They demonstrated detection limits of ~ 500 g m^{-2} at distances of 0.5 km.

As evident from the work above, UV-Raman spectroscopy is a highly sensitive and selective spectral probe of dilute species. The power of this approach derives from the fact that the majority of species have strong UV absorption bands and show strong resonance enhancement. Further, the UV-Raman spectra show high S/Ns due to the lack of luminescence interference for UV excitation below 250 nm.

6 BIOLOGICAL ULTRAVIOLET-RAMAN STUDIES

Major advances have occurred in UV-Raman measurements of biologically important molecules and for biological assemblies such as viruses, bacteria and algae. Over the last decade the resonance Raman enhancement profiles have been almost completely characterized for aromatic amino acids, peptide and protein amide vibrations, nucleic acids, DNA and visual pigments.

For example, excitation of tyrosine, tryptophan and phenylalanine roughly follows their UV absorption bands (Figures 9 and 10). Figure 9 shows the UV-Raman bands of tryptophan and tyrosine. All of the bands observed are symmetric ring in-plane breathing modes.

Most UV-Raman aromatic amino acid studies occur with excitation within the 220-nm S_2 absorption band of tyrosine and the S_3 absorption band of tryptophan, since excitation in their longer wavelength bands at ~ 270 nm results in weaker enhancement and interference from fluorescence.

The lifetimes of the S_1 excited state of tyrosine and the S_1/S_2 excited states of tryptophan are in the ~ 10 ns time regime. The Asher group used the fact that nanosecond

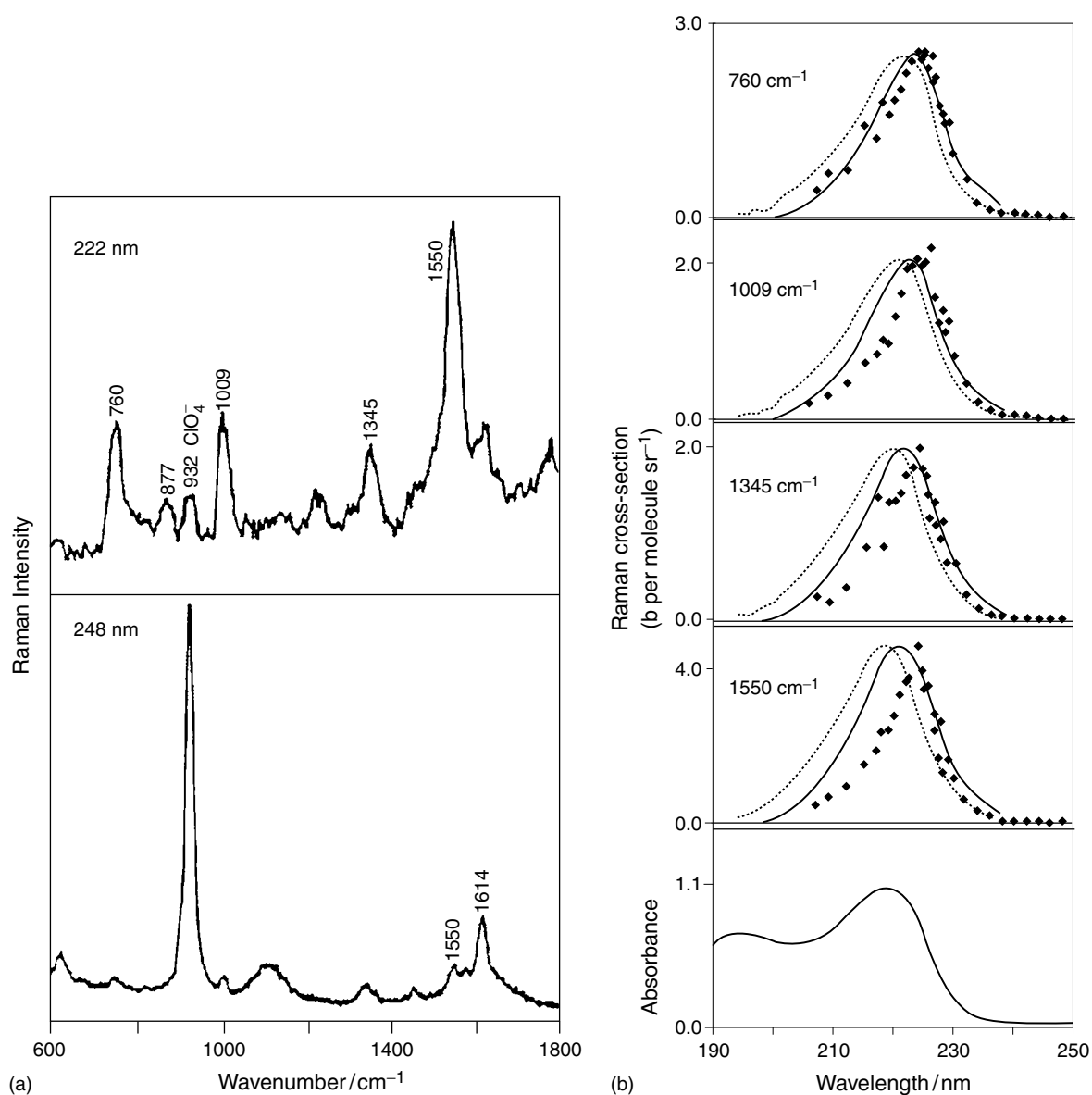


Figure 9. (a) Resonance Raman spectra of tryptophan excited at 222 and 248 nm. The 932 cm^{-1} band derives from the internal standard. Obviously, the relative intensity compared with the internal standard band increases with 222 nm excitation. This is more evident from (b) the resonance Raman excitation profiles of the vibrational modes of tryptophan. The experimental data (diamonds) are red-shifted 4 nm from the absorption maximum of the B_b transition. The broken curve represents the basic Condon transform calculation of the RREP. The solid curve is the result of introducing non-Condon coupling into the transform calculation. [Reprinted with permission from S.A. Asher, *J. Phys. Chem.*, **94**(12), 4785–6 (1990). Copyright © (1990) American Chemical Society.]

resonance laser pulse excitation occurs in a timescale similar to that required for the excited state to return back to the ground state to develop a technique called Raman saturation spectroscopy to study the photophysics of tyrosine and tryptophan residues.^{59–61}

Nanosecond UV pulsed laser excitation simultaneously excites the Raman spectra and transfers ground-state molecules into their excited states. As a result, the Raman intensities increase sublinearly with the excitation energy. Thus, the dependence of the Raman intensity on the incident

pulse energy monitors depletion of the ground state and can determine the tyrosine and tryptophan T_1 ground state recovery rates. These Raman saturation measurements were able to measure picosecond and nanosecond Forster transfer rates from tyrosine to tryptophan in peptides, and to the heme group in heme proteins. These measurements complement fluorescence lifetime measurements, and are unique in that they can measure tyrosine excited-state relaxation, in the common cases where tyrosine does not fluoresce, but transfers its energy to tryptophan.

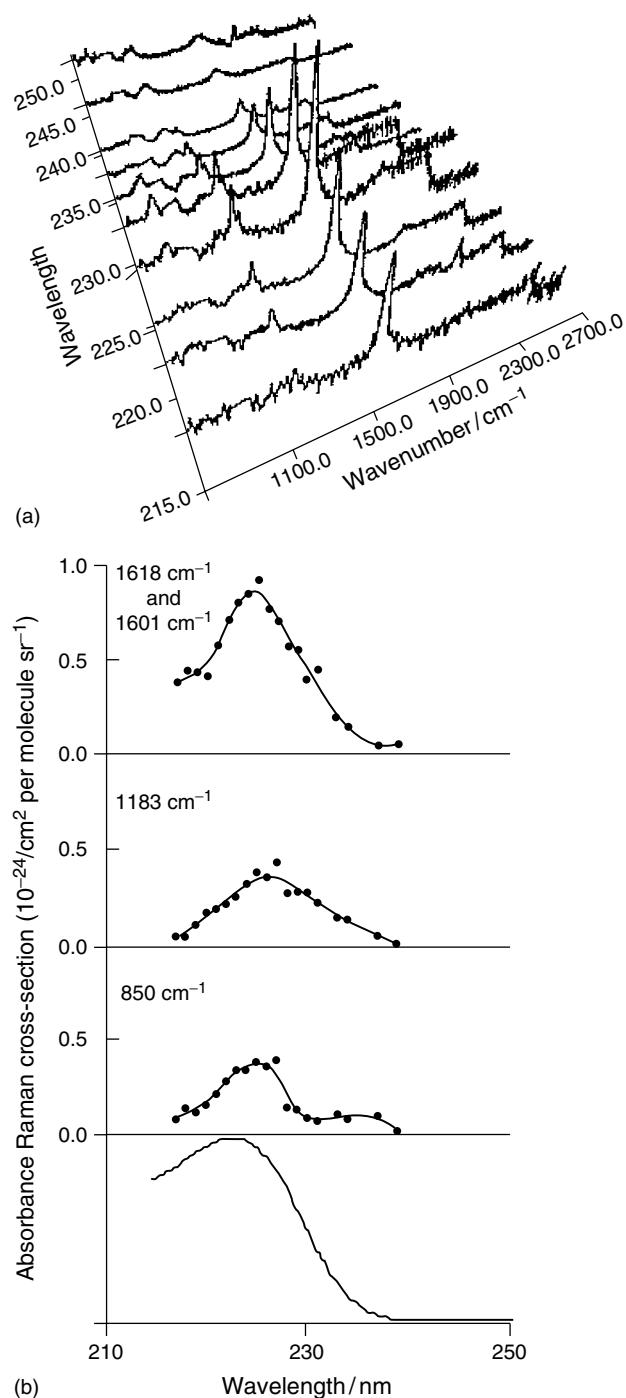


Figure 10. (a) Zwitterionic tyrosine (pH 6.0) Raman spectra excited between 217 and 250 nm. The strongest band is the 1620 cm^{-1} ring breathing mode. (b) Zwitterionic tyrosine (pH 6.0) absorption spectrum and the total differential Raman cross-section excitation profiles. [Reprinted with permission from S.A. Asher, *J. Am. Chem. Soc.*, **110**(4), 1007–8 (1998). Copyright © (1998) American Chemical Society.]

Numerous UV-Raman studies have taken advantage of the strong, selective enhancement of the tyrosine and tryptophan in proteins with $\sim 230\text{-nm}$ excitation. UV-Raman

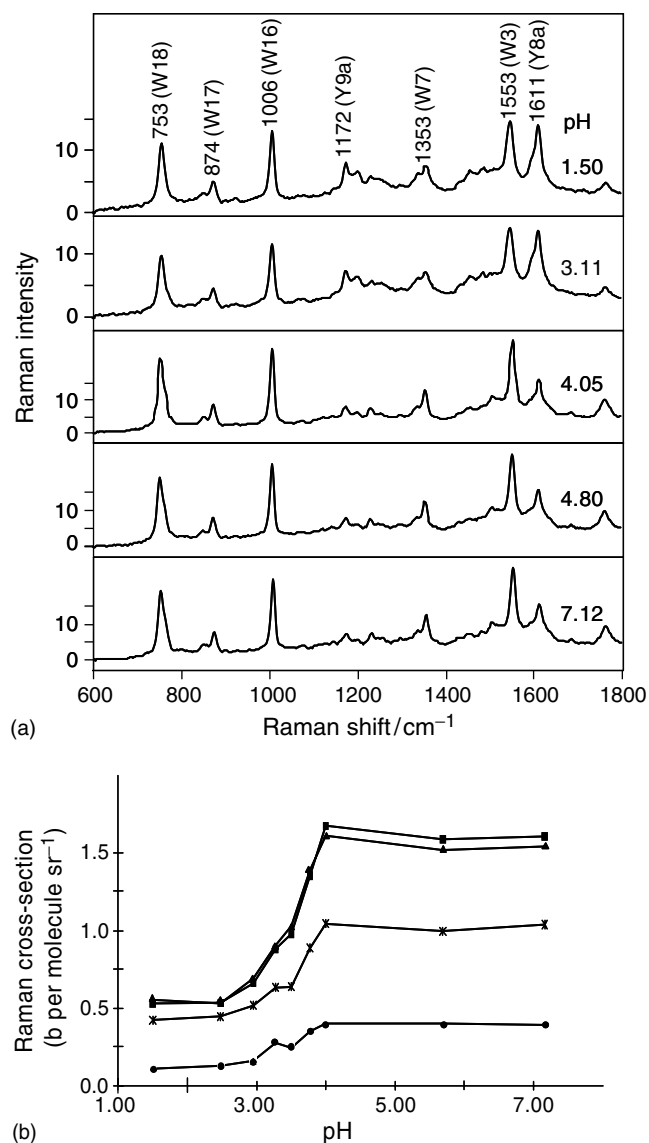


Figure 11. (a) 229-nm excited Raman spectra of horse aquometmyoglobin at various pH values.^{65,66} (b) pH dependence of 229-nm excited myoglobin tryptophan band intensities. The 500 cm^{-1} water band was used as an internal standard to determine the Raman cross-sections. \blacktriangle , W18 759 cm^{-1} , 0.574; \bullet , W17 879 cm^{-1} , 0.130; \blacksquare , W16 1012 cm^{-1} , 0.509; \times , W31 551 cm^{-1} , 0.383 b per molecule sr^{-1} . [Reprinted with permission from S.A. Asher, *Biochemistry*, **37**(9), 2868 (1998). Copyright © (1998) American Chemical Society.]

studies of tyrosine and tryptophan Raman cross-sections and their vibrational frequencies can monitor exposure of the aromatic ring side chain to the aqueous environment⁶² and the hydrogen bonding of these residues.⁶³

For example, Figure 11(a) shows the dependence of the 229-nm excited Raman spectra of horse aquomyoglobin as a function of pH.^{64–66} As the pH decreases, the intensity of the tryptophan bands at 1611, 1353, 1006, 879 and 753 cm^{-1} decreases (Figure 11b). This signals unfolding of

the A helix, which contains the two myoglobin tryptophan residues. The cross-section changes are consistent with the exposure to the tryptophan residues to the aqueous environment. The tyrosine Raman cross-sections do not change, indicating a lack of conformational changes of the helices that contain the tyrosine residues.

Excitation of proteins and peptides with ~ 205 -nm excitation selectively excites the peptide backbone amide vibrations (Figure 12). With great similarity to the enhancement in NMA (Figure 5), the protein spectra show large enhancements for the amide II and III bands and weaker enhancement of the amide I band. By examining a library of proteins we calculated⁶⁴ the Raman spectra contributed by the pure α -helix, β -sheet and random coil conformations (Figure 13).

These basis spectra demonstrate strong enhancement of the amide III (1267 cm^{-1}), amide II (1560 cm^{-1}), C_{α} -H bending (1386 cm^{-1}) and amide I (1665 cm^{-1}) in the unordered or random coil form. The amide III band is downshifted in the β -sheet form, while the C_{α} -H bending band is broadened. The amide III band is upshifted and the C_{α} -H bending mode disappears in the α -helix conformation, which shows a strong amide I band at lower frequency.

Linear fitting of these basis spectra to the observed protein and peptide Raman spectra can be used to determine the protein and peptide solution secondary structure. UV-Raman is now arguably the most sensitive method to determine dilute solution secondary structure.

Combining the information obtained from 206-nm excitation of the amide bands with information obtained from 229-nm excitation of the aromatic amino acid bands makes it possible to spatially resolve unfolding of particular segments of proteins and peptides. For example, a 206-nm study of the acid denaturation of myoglobin⁶⁵ and apomyoglobin⁶⁶ determined the pH dependence of the protein α -helical content, while a study at 229 nm found that the tyrosine environment remained intact as the protein unfolded. In contrast, in myoglobin both tryptophan residues (on the A helix) became fully solvent exposed with a pK_a of 3.5 (Figure 11). These data demonstrated that only the G and H helix remained intact by pH 2. In contrast, for apomyoglobin this study demonstrated a three-stage acid unfolding where the A helix underwent two-stage melting.

These results were used to create a model for myoglobin denaturation where helices in the heme pocket melted upon removal of the heme in apomyoglobin. As the pH decreased

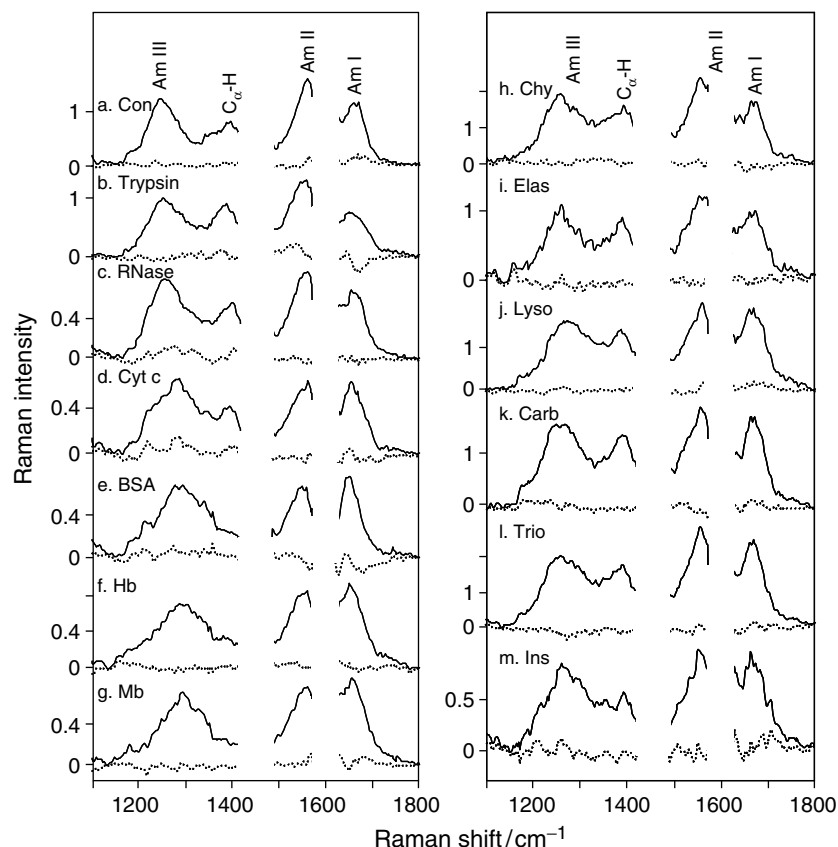


Figure 12. 206.5-nm excited measured protein Raman spectra at pH 7.0 water used for modeling the spectra and their residuals calculated as the difference between the measured and calculated spectra.

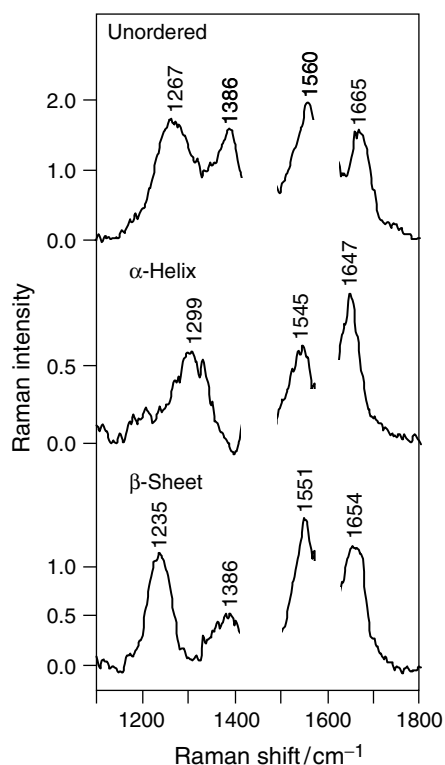


Figure 13. Calculated pure secondary structure Raman spectra (PSSRS) obtained from aqueous solution 206.5-nm protein Raman spectra. The regions around 1610 and 1450 cm^{-1} are excluded due to interference from aromatic amino acid ring vibrations and side-chain vibrations.

the A helix melted in two stages and by pH 2 the structure of myoglobin and apomyoglobin became identical.

Transient UV-Raman measurements are a powerful tool for studying protein dynamics. An important biological target for these studies is the development of a molecular level understanding of the mechanism of hemoglobin oxygen binding. Hemoglobin enhances oxygen transport by altering the heme ligand affinity of one oxygen binding subunit in response to oxygen binding by another subunit. The Spiro⁶⁷ and Kitagawa groups³⁴ used nanosecond visible excitation to partially photolyze the carbon monoxide ligand off the heme in carbonmonoxy hemoglobin. They then examined changes in the aromatic amino acid sidechain spectra with delayed nanosecond $\sim 230\text{-nm}$ excitation pulses. These studies were able to resolve hydrogen bonding changes of a functionally important tyrosine residue at the hemoglobin subunit interface that appears to serve as the conduit for actuating the protein cooperative structural changes that alter the hemoglobin subunit ligand affinities.

The Asher group has been utilizing UV-Raman to probe the early stages of protein and peptide unfolding. They developed a T-jump transient UV-Raman technique for studying the first steps in protein folding.^{17,68} Two YAG lasers were used to excite peptide and protein solutions. The

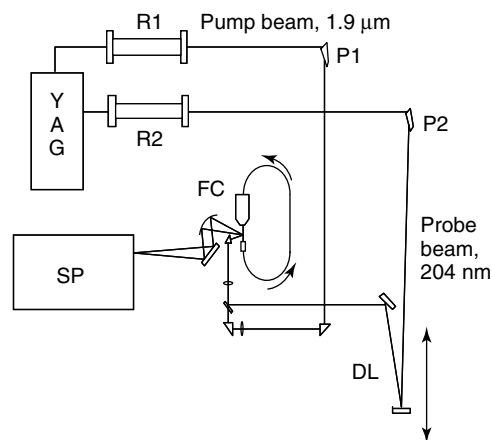


Figure 14. The T-jump spectrometer consists of a Nd:YAG laser (YAG), two H_2 Raman shifters (R1 and R2), a thermostated flow cell sample circulator (FC), and a subtractive double monochromator with a solarblind ICCD detector (SP). The heating pump beam is obtained by Raman shifting the YAG fundamental in H_2 to $1.9\text{ }\mu\text{m}$ (first Stokes). The probe beam is obtained by Raman shifting the YAG third harmonic to 204 nm (fifth anti-Stokes). The time delays between the pump and probe pulses are provided by the variable delay line (DL).

$1.06\text{ }\mu\text{m}$ fundamental of the YAG was Stokes shifted one harmonic in hydrogen to generate $1.9\text{ }\mu\text{m}$ IR light, which was absorbed by water to generate a T-jump. This T-jump was followed by a delayed 204-nm pulse to excite the amide vibrations. The 204-nm pulse was generated by shifting the 355-nm third harmonic of the YAG 5 anti-Stokes harmonics in hydrogen (Figure 14). The first applications of this transient spectrometer was to examine the dynamics of peptide unfolding of the 21 amino acid residue mainly polyalanine peptide AP. This peptide is mainly α -helical at room temperature and unfolds completely by 50°C to the random coil form. Figure 14 shows the temperature dependence of the 204-nm UV-Raman spectra. The spectra evolve with temperature, showing a downshift in the amide III frequency and an increased $\sim 1400\text{ cm}^{-1}$ C_αH bending band intensity. These changes could have been analyzed with the basis spectra of Figure 13 to calculate the peptide secondary structure at any delay time. However, we utilized α -helix and random coil basis spectra we independently calculated for AP (Figure 15). These AP α -helix and random coil basis spectra are much narrower than those of the proteins since AP is almost an oligopeptide. Steady-state UV-Raman measured melting curves accurately determined the temperature dependence of the α -helical composition; UV-Raman measurements appear to be more linear in α -helix composition than is CD spectroscopy.

The transient UV-Raman spectra (Figure 15) indicate that negligible conformational changes occur at short delay ($<20\text{ ns}$). The short time spectral changes were shown to

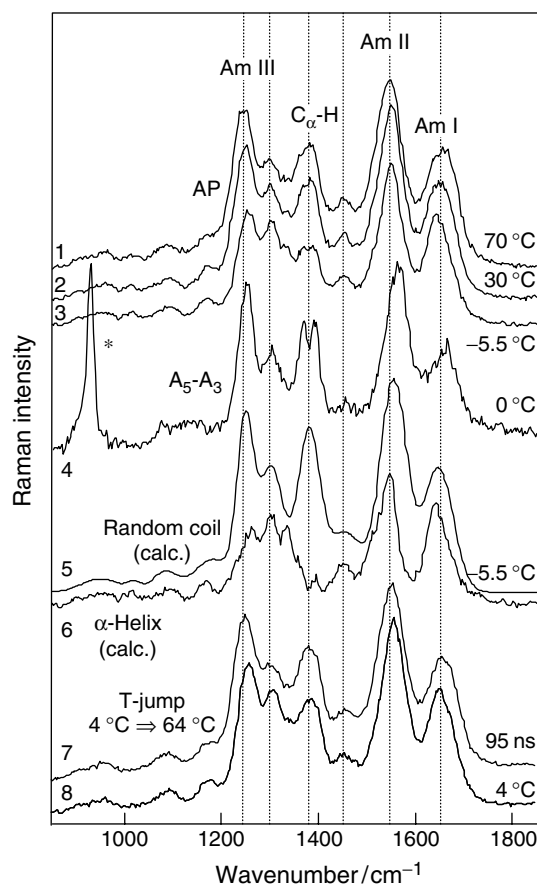


Figure 15. Comparison between steady-state and time-resolved 204-nm UVRS of AP ($\sim 15 \text{ mg mL}^{-1}$). AP UVRS measured at (1) $+70^\circ\text{C}$, (2) $+30^\circ\text{C}$, and (3) $+5.5^\circ\text{C}$. (4) The 0°C UV-Raman difference spectrum between penta-alanine and tri-alanine; (5) pure random coil ($T = -5.5^\circ\text{C}$); and (6) α -helix ($T = -5.5^\circ\text{C}$) basis Raman spectra of AP (see text). Transient UVRS of AP measured at (7) 95 ns after a T-jump of $\sim 60^\circ\text{C}$ and (8) a static UVRS of AP at 4°C in the absence of a T-jump.

result only from a temperature jump of the static AP initial conformations. The AP peptide unfolds at room temperature with a ~ 200 -ns relaxation time.

The measured temperature dependences of the relaxation rates were combined with the measured temperature dependences of the equilibrium constants for unfolding in order to calculate the Arrhenius activation barriers. The unfolding activation barrier energy was $\sim 8 \text{ kcal mol}^{-1}$, a value that is similar to that determined by other methods. In contrast, the folding barrier showed a negative activation barrier, which clearly indicates that even this simple peptide system (where amide conformations change only between α -helix and random coil states) cannot be considered as a simple two-state equilibrium. In fact, the energy landscape is highly complex and a more sophisticated view of the unfolding is required.

In fact, UV-Raman measurements are providing a much more detailed examination of the unfolding mechanism.

The peptide has been isotopically labeled at each amino acid along the chain by deuterating the C_α position. The amide III band is significantly blue-shifted for the deuterated derivative, while the C_α bending vibration is absent. Thus, the difference spectra between the selectively labeled peptide and the fully hydrogenated peptide selectively monitors the secondary structure and dynamics of the labeled position. Future studies will examine the dynamics of these particular sites due to unfolding induced by a T-jump. The results of these studies will test the existing theoretical models, which predict the dynamics and mechanisms of α -helix melting.

Numerous other proteins have recently been subjects of UV-Raman investigations. An important group is the visual pigments. These species, such as rhodopsin and bacteriorhodopsin, were extensively investigated by visual Raman measurements with the objective of determining the photochemistry of the retinal pigment. Further investigations using UV-Raman are examining the coupling of retinal photochemistry with the aromatic amino acid environments.^{69,70}

While this review has emphasized structural and dynamical studies of proteins, numerous other studies have focused on nucleic acids and DNA.⁷¹ The field is rapidly expanding with numerous reports appearing monthly.

A number of groups are attempting to use UV-Raman to examine more complex biological systems such as cells, viruses and tissues. For example, the Nelson group has examined the utility of UV-Raman to study microorganisms,^{71,72} while the Thomas group has examined DNA and proteins in viruses.⁷³ Sureau *et al.*,⁷⁴ Richards-Kortum *et al.*⁷⁵ and Feld *et al.*^{71,76} have attempted to differentiate cancerous from noncancerous cells.

7 CONCLUSIONS

Obviously, the field of UV-Raman is flourishing. The major limitation to the use of UV-Raman is the high cost of instrumentation, especially the laser sources. Further, until most recently, UV-Raman instruments were commercially unavailable.

However, continuing advances in laser technology are rapidly decreasing the cost of UV excitation sources and commercial instruments are emerging. The field of UV-Raman is expected to dramatically expand its scope as more fundamental and applied studies demonstrate its high information content. Resonance Raman spectroscopy is extraordinarily sensitive to molecular structural details since it directly probes the coupling of molecular vibrations to the frontier electrons involved in the UV electronic transitions of a molecule. The selectivity of resonance excitation

allows the spectroscopist to focus on the dynamics of particular frontier electrons of the analyte species of interest. Resonance enhancement allows studies of low concentrations of analyte. The ultimate limitation in UV-Raman measurements is the resistance of the sample to photochemistry induced by the UV excitation. To date this has not posed an insurmountable problem to any UV-Raman investigation to my knowledge.

ACKNOWLEDGMENTS

I am pleased to acknowledge the excellent work of the post-doctorate and graduate students who have developed UV-Raman in my laboratories. I would also like to acknowledge the long-term support of NIH in the development of UV-Raman through grant GM30741.

ABBREVIATIONS AND ACRONYMS

CVD	Chemical Vapor Deposition
CW	Continuous Wave
Nd:YAG	Neodymium Doped Yttrium Aluminum Garnet
NMA	N-Methylacetamide
PAH	Polycyclic Aromatic Hydrocarbon
PSSRS	Pure Secondary Structure Raman Spectra

REFERENCES

- D.A. Long, 'Raman Spectroscopy', McGraw-Hill, New York (1977).
- S.A. Asher, *Ann. Rev. Phys. Chem.*, **39**, 537 (1988).
- I. Harada and H. Takeuchi, 'Raman and Ultraviolet Resonance Raman Spectra of Proteins and Related Compounds', in "Spectroscopy of Biological Systems", eds R.T. Clark and R.E. Hester, J. Wiley & Sons, New York (1986).
- B. Hudson and L. Mayne, *Methods Enzymol.*, **130**, 331 (1986).
- P.A. Harmon and S.A. Asher, *J. Chem. Phys.*, **88**, 2925 (1988).
- F.A. Miller and G.B. Kauffman, *J. Chem. Educ.*, **66**, 795 (1989).
- T.C. Streckas and T.G. Spiro, *Biochim. Biophys. Acta*, **263**, 830 (1972).
- T.G. Spiro, G. Smulevich and C. Su, *Biochemistry*, **29**, 4497 (1990).
- S.A. Asher, *Methods Enzymol.*, **76**, 372 (1981).
- R. Mathies, S.O. Smith and I. Palings, in "Biological Applications of RS", ed. T.G. Spiro, J. Wiley & Sons, New York, Vol. II (1987).
- B. Chase, *Anal. Chem.*, **59**, 881A (1987).
- S.A. Asher and C.R. Johnson, *Science*, **225**, 311 (1984).
- J.M. Dudik, C.R. Johnson and S.A. Asher, *J. Chem. Phys.*, **82**, 1732 (1985).
- C.M. Jones and S.A. Asher, *J. Chem. Phys.*, **89**, 2649 (1988).
- S.A. Asher, C.R. Johnson and J. Murtaugh, *J. Rev. Sci. Instrum.*, **54**, 1657 (1983).
- L.D. Ziegler and B.S. Hudson, *J. Chem. Phys.*, **74**, 982 (1981).
- I.K. Lednev, A.S. Karnoup, M.C. Sparrow and S.A. Asher, *J. Am. Chem. Soc.*, **121**, 8074 (1999).
- C.M. Jones, V.L. DeVito, P.A. Harmon and S.A. Asher, *Appl. Spectrosc.*, **41**, 1268 (1987).
- K.P.J. Williams and D.J. Klenerman, *Raman Spectrosc.*, **23**, 191 (1992).
- T.L. Gustafson, *Opt. Commun.*, **67**, 53 (1988).
- X. Zhao, R. Chen, C. Tengroth and T.G. Spiro, *Appl. Spectrosc.*, **53**, 1200 (1999).
- S.A. Asher, R.W. Bormett, X.G. Chen, D.H. Lemmon, N. Cho, P. Peterson, M. Arrigoni, L. Spinelli and J. Cannon, *Appl. Spectrosc.*, **47**, 628 (1993).
- J.S.W. Holtz, R.W. Bormett, Z. Chi, N. Cho, X.G. Chen, V. Pajcini, S.A. Asher, L. Spinelli, P. Owen and M. Arrigoni, *Appl. Spectrosc.*, **50**, 1459 (1996).
- M.C. Sparrow, J. Jackovitz, C.H. Munro, W. Hug and S.A. Asher, *Appl. Spectrosc.*, **55**, 66 (2001).
- V. Pajcini, C.H. Munro, R.W. Bormett and S.A. Asher, *Appl. Spectrosc.*, **51**, 81 (1997).
- Y.P. Zhang and L.D. Ziegler, *J. Phys. Chem.*, **93**, 6665 (1989).
- L.D. Ziegler, *J. Chem. Phys.*, **86**, 1703 (1987).
- D.L. Phillips and A.B. Myers, *J. Chem. Phys.*, **95**, 226 (1991).
- D.L. Phillips, A.B. Myers and J.J. Valentini, *J. Phys. Chem.*, **96**, 2039 (1992).
- B. Li and A.B. Myers, *J. Chem. Phys.*, **94**, 2458 (1991).
- X. Ci and A.B. Myers, *Chem. Phys. Lett.*, **158**, 263 (1989).
- R.J. Sension and B.S. Hudson, *J. Chem. Phys.*, **90**, 1377 (1989).
- L.D. Ziegler and B.S. Hudson, *J. Chem. Phys.*, **79**, 1134 (1983).
- S.A. Asher, *Anal. Chem.*, **65**, 59A, 201A (1993).
- X.G. Chen, R. Schweitzer-Stenner, S. Krimm, N. Mirkin and S.A. Asher, *J. Am. Chem. Soc.*, **117**, 2884 (1995).
- S.A. Asher, Z. Chi and P. Li, *J. Raman Spectrosc.*, **29**, 927 (1998).
- X.G. Chen, P. Li, J.S.W. Holtz, Z. Chi, V. Pajcini, S.A. Asher and L.A. Kelly, *J. Am. Chem. Soc.*, **118**, 9705 (1996).
- V. Pajcini and S.A. Asher, *J. Am. Chem. Soc.*, **121**, 10942 (1999).
- V. Pajcini, X.G. Chen, R.W. Bormett, S.J. Geib, P. Li, S.A. Asher and E.G. Lidiak, *J. Am. Chem. Soc.*, **118**, 9716 (1996).
- S.A. Asher, *Anal. Chem.*, **56**, 720 (1984).

41. C.R. Johnson and S.A. Asher, *Anal. Chem.*, **56**, 2258 (1984).
42. S.A. Asher and C.M. Jones, 'UV Resonance Spectroscopy: A New Technique for Speciation of Aromatics in Complex Matrices', in "New Applications of Analytical Techniques to Fossil Fuels", eds M. Perry and H. Retcofsky, ACS Symposium Series 31, American Chemical Society, Washington, DC, 170–180 (1986).
43. R. Rummelfanger, S.A. Asher and M.B. Perry, *Appl. Spectrosc.*, **42**, 267 (1988).
44. C. Li and P.C. Stair, *Catalysis Today*, **33**, 353 (1997).
45. Y.T. Chua and P.C. Stair, *J. Catal.*, **196**, 66 (2000).
46. R.W. Bormett, S.A. Asher, R.E. Witkowski, W.D. Partlow, R. Lizewski and F. Pettit, *J. Appl. Phys.*, **77**, 5916 (1995).
47. C.D. Zuiker, A.R. Krauss, D.M. Gruen, J.A. Carlisle, L.J. Terminello, S.A. Asher and R.W. Bormett, *Mater. Res. Soc. Symp. Proc.*, **437**, 211 (1996).
48. V.I. Merkulov, J.S. Lannin, C.H. Munro, S.A. Asher, V.S. Veerasamy and W.I. Milne, *Phys. Rev. Lett.*, **78**, 4869 (1997).
49. M.D. Ray, A.J. Sedlacek and M. Wu, *Rev. Sci. Instrum.*, **71**, 3485 (2000).
50. M. Wu, M. Ray, K.H. Fung, M.W. Ruckman, D. Harder and A.J. Sedlacek, *Appl. Spectrosc.*, **54**, 800 (2000).
51. S.A. Asher, M. Ludwig and C.R. Johnson, *J. Am. Chem. Soc.*, **108**, 3186 (1986).
52. C.R. Johnson, M. Ludwig and S.A. Asher, *J. Am. Chem. Soc.*, **108**, 905 (1986).
53. M. Ludwig and S.A. Asher, *J. Am. Chem. Soc.*, **110**, 1005 (1988).
54. J. Sweeney and S.A. Asher, *J. Phys. Chem.*, **94**, 4784 (1990).
55. C.R. Johnson, M. Ludwig, S. O'Donnell and S.A. Asher, *J. Am. Chem. Soc.*, **106**, 5008 (1984).
56. C. Su, Y. Wang and T.G. Spiro, *J. Raman Spectrosc.*, **21**, 8179 (1990).
57. S. Fodor, R. Copeland, C. Grygon and T.G. Spiro, *J. Am. Chem. Soc.*, **111**, 5509 (1989).
58. R. Rava and T.G. Spiro, *J. Phys. Chem.*, **89**, 1856 (1985).
59. J. Teraoka, P.A. Harmon and S.A. Asher, *J. Am. Chem. Soc.*, **112**, 2892 (1990).
60. P.A. Harmon, J. Teraoka and S.A. Asher, *J. Am. Chem. Soc.*, **112**, 8789 (1990).
61. J. Sweeney, P.A. Harmon, S.A. Asher, C.M. Hutnik and A.G. Szabo, *J. Am. Chem. Soc.*, **113**, 7531 (1991).
62. Z. Chi and S.A. Asher, *J. Phys. Chem. B*, **102**, 9595 (1998).
63. M. Matsuno and G. Takeuchi, *Bull. Chem. Soc. Jpn.*, **71**(4), 851 (1998).
64. Z. Chi, X.G. Chen, J.S.W. Holtz and S.A. Asher, *Biochemistry*, **37**, 2854 (1998).
65. Z. Chi and S.A. Asher, *Biochemistry*, **37**, 2865 (1998).
66. Z. Chi and S.A. Asher, *Biochemistry*, **38**, 8196 (1999).
67. D. Wang, X. Zhao and T.G. Spiro, *J. Phys. Chem. A*, **104**, 4149 (2000).
68. I. Lednev, A. Karnoup, M. Sparrow and S.A. Asher, *J. Am. Chem. Soc.*, **123**, 2388 (2001).
69. G.G. Kochendoerfer, S. Kaminaka and R.A. Mathies, *Biochemistry*, **36**, 13 153 (1997).
70. S. Hashimoto, K. Obata, H. Takeuchi, R. Needleman and J.K. Lanyi, *Biochemistry*, **36**, 11 583 (1997).
71. E.B. Hanlon, R. Manoharan, T.-W. Koo, K.E. Shafer, J.T. Motz, M. Fitzmaurice, J.R. Kramer, I. Itzkan, R.R. Dasari and M.S. Feld, *Phys. Med. Biol.*, **45**, 1 (2000).
72. E. Ghiamati, R. Manoharan, W.H. Nelson and J.F. Sperry, *Appl. Spectrosc.*, **46**, 357 (1992).
73. Z.Q. Wen and G.J. Thomas Jr, *Biochemistry*, **39**, 146 (2000).
74. F. Sureau, L. Chinsky, C. Amirand, J.P. Ballini, M. Duquesne, A. Laigle, P.Y. Turpin and P. Vigny, *Appl. Spectrosc.*, **44**, 1047 (1990).
75. Y. Yazdi, N. Ramanujam, R. Lotan, M.F. Mitchell, W. Hittelman and R. Richards-Kortum, *Appl. Spectrosc.*, **53**, 82 (1999).
76. N.N. Boustany, J.M. Crawford, R. Manoharan, R.R. Desara and M.S. Feld, *Lab. Invest.*, **79**(10), 1201 (1999).